

Heat percolation in many-body flatband localizing systems

I. Vakulchyk,^{1,2,*} C. Danieli,^{3,†} Alexei Andreanov,^{1,2,‡} and S. Flach^{1,2,§}

¹Center for Theoretical Physics of Complex Systems, Institute for Basic Science (IBS), Daejeon 34126, Republic of Korea

²Basic Science Program, Korea University of Science and Technology (UST), Daejeon, Korea, 34113

³Max Planck Institute for the Physics of Complex Systems, Dresden D-01187, Germany

(Dated: October 7, 2021)

Translationally invariant finetuned single-particle lattice Hamiltonians host flat bands only. Suitable short-range many-body interactions result in complete suppression of particle transport due to local constraints and Many-Body Flatband Localization. Heat can still flow between spatially locked charges. We show that heat transport is forbidden in dimension one. In higher dimensions heat transport can be unlocked by tuning filling fractions across a percolation transition for suitable lattice geometries. Transport in percolation clusters is additionally affected by effective bulk disorder and edge scattering induced by the local constraints, which work in favor of arresting the heat flow. We discuss explicit examples in one and two dimensions.

Introduction — The breaking of ergodicity in interacting quantum many-body systems, known as many-body localization (MBL), is an important open problem and active topic of research. The first studies [1–5] showed that MBL and the exponential suppression of any transport arise in one-dimensional interacting systems from the interplay of random fields and interactions. While the original MBL framework has been widely developed both theoretically and experimentally [6, 7], the need for random fields as a key element for MBL has been later relaxed as MBL features have been found in a variety of systems without disorder [8–13] – particularly, in interacting systems featuring an extensive number of local constraints [14–19]. Computationally, interacting quantum systems face an exponential divergence in complexity over the system size, which limits most of numerical efforts to 1D. This, and the lack of analytically treatable models and methods, renders the crucial quest for MBL in higher-dimensional networks particularly challenging. Indeed, while signatures of MBL in 2D systems have been reported [20, 21], it has also been shown that in $D > 1$ the MBL regime is possibly unstable and destabilised in the long time limit [22].

In this Letter, we study the transport features of disorder-free many-body systems which are based on Hamiltonian networks completely lacking single-particle dispersion. In particular, we relate the existence of phase transitions between conducting and insulating regimes to the lattice profile and its dimensionality. In translationally invariant lattices, the lack of single-particle dispersion in *e.g.* one Bloch band typically results in a macroscopically degenerate set of eigenstates, all spatially compact (CLS) [23–25]. Hence, a complete lack of dispersion – i.e. all Bloch bands are flat (ABF) [26–28] – results in the absence of extended states and strict single-particle confinement in the network. Flatband networks are increasingly permeating the quantum many-body field. Indeed, single-particle CLS have been extended to many-body CLS [29–31], while quantum scars [32–34] and MBL-like dynamics [35–37] have been reported

very recently in flatband lattices. But more importantly, it has been shown that fine-tuning of the interaction in ABF networks induces an extensive set of local constraints which completely suppress charge transport in any spatial dimension – a phenomenon called many-body flatband localization (MBFBL) [38–40]. We focus on MBFBL networks, and by recasting them into a site-percolation problem we show that the structure of the Hilbert space undergoes a percolation transition upon tuning the filling fraction. Percolation approaches have been formerly employed to study MBL phenomena – *e.g.* Refs. [41–43], and more recently [19]. One of our main findings is that the critical value depends only on the lattice geometry and dimensionality, but not on particular realizations of the Hamiltonian terms – thus indicating universality. More specifically, such transitions are absent and any transport is suppressed in all 1D networks, whereas in $D \geq 2$ the presence of the transition depends on the MBFBL geometry – highlighting high-dimensional many-body systems where transport vanishes at any filling fraction. Additionally, we found that in the conducting phases predicted by percolation, the local constraints hurdle and potentially stop transport by generating effective bulk and edge disorders.

Setup — We study interacting many-body systems whose Hamiltonians consist of D -dimensional networks with ν strictly flat energy bands equipped with fine-tuned two-body interactions. Without loss of generality we consider spinless fermions, and following the scheme outlined in Ref. [38] we consider a set of Hamiltonians written as

$$\hat{H} = \hat{H}_{\text{sp}} + V \hat{H}_{\text{int}} \\ = \sum_{\mathbf{l}} \hat{C}_{\mathbf{l}}^{\dagger T} H_0 \hat{C}_{\mathbf{l}} + V \sum_{\langle \mathbf{l}_1, \mathbf{l}_2 \rangle} \sum_{a,b} J_{a,b}^{\mathbf{l}_1, \mathbf{l}_2} \hat{n}_{\mathbf{l}_1, a} \hat{n}_{\mathbf{l}_2, b}, \quad (1)$$

where in \hat{H}_{sp} the fermionic annihilation (creation) operators $\hat{c}_{\mathbf{l}, a}$ ($\hat{c}_{\mathbf{l}, a}^{\dagger}$) have been grouped in ν -dimensional vectors $\hat{C}_{\mathbf{l}}$ ($\hat{C}_{\mathbf{l}}^{\dagger}$), while H_0 is a Hermitian matrix, \mathbf{l} is a D -dimensional multi-index and a, b label sites in unit cells. In Ref. 38, this representation of \hat{H}_{sp} has been named

semi-detangled since $\hat{\mathcal{H}}_{\text{sp}}$ consists of decoupled unit cells of ν lattice sites each, whose profile is defined by H_0 . The interaction $\hat{\mathcal{H}}_{\text{int}}$ is set as products of particle-number operators $\hat{n}_{1,a} = \hat{c}_{1,a}^\dagger \hat{c}_{1,a}$. The multi-indices $\langle \mathbf{l}_1, \mathbf{l}_2 \rangle$ account for neighboring unit cells reflecting the geometry of the interaction network, while the coefficients $J_{a,b}^{\mathbf{l}_1, \mathbf{l}_2}$ define the interaction between cells \mathbf{l}_1 and \mathbf{l}_2 .

The addition of a fine-tuned density-density interaction $\hat{\mathcal{H}}_{\text{int}}$ to the semi-detangled all-band-flat networks $\hat{\mathcal{H}}_{\text{sp}}$ in Eq. (1) results in strict particle localization – a phenomenon labeled Many-Body Flatband Localization (MBFBL). Indeed, the local operators $\hat{I}_1 = \sum_{a=1}^\nu \hat{n}_{1,a}$ that count the number of particles within each unit cell, commute with $\hat{\mathcal{H}}$ (1) and prohibit charge transport. The Hilbert space decomposes into dynamically independent subspaces characterized by the eigenvalues of $\{\hat{I}_1\}$. In general, the local conserved quantities \hat{I}_1 do not forbid global heat transport, since particles confined to neighboring unit cells might still exchange energy locally via the interaction $\hat{\mathcal{H}}_{\text{int}}$ [44]. However the local heat exchange vanishes if at least one of the two cells coupled by $\hat{\mathcal{H}}_{\text{int}}$ is either empty or full, i.e. $\hat{I}_1 = \{0, \nu\}$. Consequently unit cells of Eq. (1) split according to their occupation number into *blocking* (empty/full cell, $\hat{I}_1 = \{0, \nu\}$) or *conducting* (all the other cases, $\hat{I}_1 \neq \{0, \nu\}$). The impact of blocking cells on the global heat transport in Eq. (1) depends on the network geometry encoded by $\langle \mathbf{l}_1, \mathbf{l}_2 \rangle$, its spatial dimension D , the number of single particle flatbands ν , and the filling fraction δ .

One-dimensional case — In 1D MBFBL networks (1), a single blocking unit cell acts as a bottleneck, strictly disconnecting left and right parts of a given state of the Hilbert space and completely removing any global heat transport. Consequently, subspaces labelled by $\{\hat{I}_1\}$ are separated into (i) *conducting channels* where every unit cell is conducting (hence, there exists a continuous path along heat-exchanging units which connect opposite ends of the system), and (ii) *non-conducting states* where at least one unit cell is blocking. Within a non-conducting state, blocking cells separate contiguous conducting unit cells, *conducting islands*, where heat transport is possible although non-global. The existence of conducting channels – and the possibility of heat transport – in 1D networks (1) is controlled by the filling fraction δ . For $1/\nu \leq \delta \leq (\nu - 1)/\nu$ conducting and non-conducting channels coexist, otherwise only non-conducting states are present.

The $\nu = 2$ case is the minimal testbed setup. In this case, conducting channels are only present at precisely filling fraction $\delta = 0.5$ ($\hat{I}_1 = 1$ in all cells). An example network (1) is shown in Fig. 1(a), the corresponding Hamiltonian $\hat{\mathcal{H}}$ reads

$$\hat{\mathcal{H}} = \sum_l (\hat{a}_l, \hat{b}_l)^\dagger \begin{pmatrix} s & t \\ t & s \end{pmatrix} \begin{pmatrix} \hat{a}_l \\ \hat{b}_l \end{pmatrix} + V \sum_l \hat{n}_{b,l} \hat{n}_{a,l+1}, \quad (2)$$

where $\hat{a}_l, \hat{b}_l (\hat{a}_l^\dagger, \hat{b}_l^\dagger)$ are the fermionic annihilation (cre-

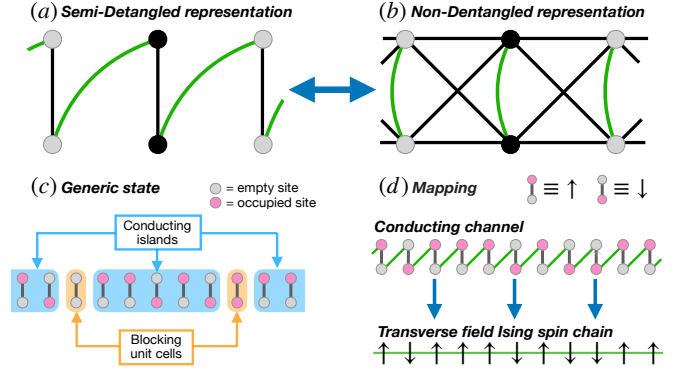


FIG. 1. (a) One dimensional $\nu = 2$ MBFBL network Eq. (2) with $\hat{\mathcal{H}}_{\text{sp}}$ (black lines) and $\hat{\mathcal{H}}_{\text{int}}$ (green curves). The black circles indicate the unit cell choice. (b) Same as (a) with $\hat{\mathcal{H}}_{\text{sp}}$ non-detangled (cross-stitch). (c) Conducting islands (blue shaded area) and blocking unit cells (orange shaded area) in a generic state of the Hilbert space of $\hat{\mathcal{H}}$. (d) Visualization of the mapping of $\hat{\mathcal{H}}$ (2) to a transverse field Ising spin chain $\hat{\mathcal{H}}_I$ (3) in the subspace of conducting channels at $\delta = 0.5$. The green horizontal line indicates the spin-interaction terms.

ation) operators, $\hat{n}_{a,l}, \hat{n}_{b,l}$ are the respective particle-number operators and s, t are onsite energies and intracell hopping respectively. Note that this network is related to the (non-detangled) cross-stitch lattice Fig. 1(b) by local unitary transformations [45], that preserve $\hat{\mathcal{H}}_{\text{int}}$ as density-density interaction [38].

A generic non-conducting state is shown in Fig. 1(c), where contiguous conducting islands are separated by blocking unit-cells. Instead, a sample conducting channel is shown in Fig. 1(d). Within the conducting channels that exist at $\delta = 0.5$, the Hamiltonian $\hat{\mathcal{H}}$ (2) maps onto a spin- $\frac{1}{2}$ transverse field Ising model [46]. The mapping is visualized in Fig. 1(d): we define local spin basis $|\uparrow\rangle \equiv \hat{a}_l |0\rangle$ (one fermion at site a) and $|\downarrow\rangle \equiv \hat{b}_l |0\rangle$ (one fermion at site b) for each unit cell l . In this representation, the onsite terms of $\hat{\mathcal{H}}$ become an identity, the hopping terms turn into σ_l^x , while the interaction reads $(1 - \hat{\sigma}_l^z)(1 + \hat{\sigma}_{l+1}^z)/4$ – where $\hat{\sigma}_l^\alpha$ are Pauli matrices. The effective spin-1/2 Hamiltonian of the conducting channels reads

$$\hat{\mathcal{H}}_I = t \sum_l \hat{\sigma}_l^x - \frac{V}{4} \sum_l \hat{\sigma}_l^z \hat{\sigma}_{l+1}^z + \frac{V}{4} (\hat{\sigma}_L^z - \hat{\sigma}_1^z), \quad (3)$$

where the last term vanishes for periodic boundary conditions [47]. Note that this mapping can also be done within individual conducting islands of nonconducting channels. In that case, the boundary term in Eq. (3) depends on whether the blocking cells at the edges of the island are empty or filled – see [48].

This mapping of $\hat{\mathcal{H}}$ (2) to the transverse field Ising chain $\hat{\mathcal{H}}_I$ (3) implies ballistic heat transport in the conducting channel [49]. However, the total dimension of nonconducting channels overpowers the dimension of the

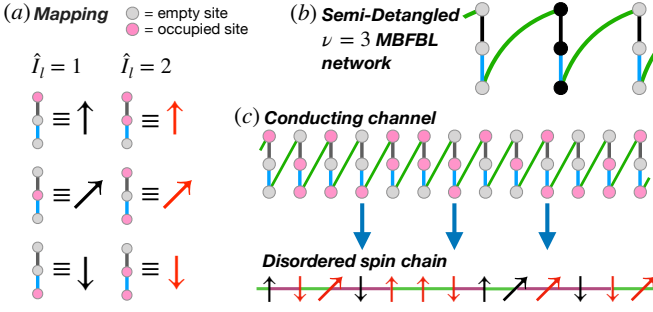


FIG. 2. (a) Mapping of conducting unit cells to spin-1 representation of $\nu = 3$ MBFBL networks separated in $\hat{I}_l = 1$ and $\hat{I}_l = 2$. Black and red colors indicate different spin field components. (b) One dimensional sample $\nu = 3$ MBFBL network Eq. (1) represented like Fig. 1(a). Blue and black lines indicate two different hoppings. (c) Recasting a conducting channel into spin representation via the mapping in (a). Green and magenta horizontal lines represent the spin interaction terms between neighboring unit cells with same or different value of \hat{I}_l respectively.

conducting channel for diverging number L of unit cells. Indeed, the size of the conducting channel is 2^L while the full Hilbert space dimension is $\mathcal{D} = \binom{2L}{L} \sim 2^{2L}/\sqrt{L}$ for large L . Consequently, the relative dimension \mathcal{R} of the conducting channel with respect to the full Hilbert space \mathcal{D} is $\mathcal{R} \sim \sqrt{L}2^{-L}$, implying an exponential suppression of heat transport for large L . Note that the eigenenergies of the conducting subspace are spread throughout the entire spectrum. These results are not specific to the testbed case Eq. (2), but apply to any choice of \hat{H}_{sp} and \hat{H}_{int} in \hat{H} in Eq. (1) that leads to MBFBL.

In general, for $\nu \geq 3$ conducting channels are present within a range of filling fractions $1/\nu \leq \delta \leq (\nu - 1)/\nu$. Similarly to the $\nu = 2$ case, the ratio \mathcal{R} between the dimension of the conducting channels and the full Hilbert space dimension decays exponentially in L , with the decay rate depending on the number of bands and the filling fraction. For example, for $\nu = 3$ the ratio scales as

$$\mathcal{R} \sim \left\{ \frac{(\delta - 1/3)^{\delta-1/3} (2/3 - \delta)^{2/3-\delta}}{\delta^\delta (1-\delta)^{1-\delta}} \right\}^{-3L}, \quad (4)$$

where the expression in the parenthesis is strictly greater than one for any $1/3 \leq \delta \leq 2/3$.

For $\nu = 3$ systems (1), conducting channels are given by $\hat{I}_l = 1, 2 \forall l$ – namely, each unit cell contains either one or two fermions. This corresponds to three degrees of freedom per unit cell, leading to a mapping onto a spin-1 model. However, the matrix H_0 in (1), that translates into local fields, takes different form for singly or doubly occupied cells [50]. Similarly, the mapping of the interaction \hat{H}_{int} depends on the filling fraction of the neighbouring unit cells \hat{I}_l, \hat{I}_{l+1} . Consequently, an inhomogeneous distribution of charges in the conducting channel generates an effective disorder in the interaction terms of the

spin-1 Hamiltonian, and possibly in its local field components (according to H_0). Such effects also persist for $\nu \geq 4$ networks where in addition to this disorder in local fields and the interactions, different possible fillings of unit cells $1 \leq \hat{I}_l \leq \nu - 1$ produce spins of different lengths – yielding an effective disorder in the spin length. All these effective disorders can hinder and potentially halt transport in conducting channels: it has been shown that disorder in the interaction can induce MBL [51]. This mapping is illustrated in Fig. 2(b) for a sample MBFBL network, that extends Eq. (2) to $\nu = 3$. The details of the mapping are schematically represented in Fig. 2(a), where black and red colors indicate the different field components of H_0 . The resulting transformation from a sample conducting channel to spin chain is visualized in Fig. 2(c), where the green and magenta horizontal lines indicate different interaction operators.

Higher dimensions — Unlike the one-dimensional case, a single blocking unit cell does not completely halt global transport in $D \geq 2$. Thus, a subspace is a *conducting channel* if there is at least one path formed by conducting cells connecting opposite sites of the network. Otherwise, a subspace is non-conducting. For finite system sizes conducting channels exist only in a limited range of filling fractions δ , which converges to the full available interval $0 < \delta < 1$ for $L \rightarrow \infty$ – e.g. for a square lattice of size L , conducting channels exist for $1/(\nu L) \leq \delta \leq (\nu L - 1)/(\nu L)$. In the infinite system size limit, let us consider a random state from the particle-number basis. The probability p for a given unit cell in the state to be conducting (e.g. nor empty $\hat{I}_1 = 0$ nor full $\hat{I}_1 = \nu$) is $p = 1 - \delta^\nu - (1 - \delta)^\nu$. However because the sampling is performed from the fermionic Hilbert space basis, the events of each of the unit cells being conducting are correlated. Nonetheless, these correlations are inversely proportional to the system size and become negligible as $L \rightarrow \infty$ (as we verify numerically below). Therefore counting the relative dimension of conducting channels \mathcal{R} with respect to the size of the Hilbert space in a network (1) is equivalent to a site-percolation problem, that is covered by the standard Bernoulli percolation theory [52] In a site-percolation problem there exists always a critical value of probability p_{cr} [53] which depends on the network geometry, such that $\mathcal{R} \xrightarrow{L \rightarrow \infty} 0$ for $p < p_{\text{cr}}$ (*non-transporting regime*) while $\mathcal{R} \xrightarrow{L \rightarrow \infty} 1$ for $p > p_{\text{cr}}$ (*transporting regime*).

In the MBFBL networks (1), the critical transition probability p_{cr} depends on the network connectivity $(\mathbf{l}_1, \mathbf{l}_2)$ that links the detangled unit cells, together with the dimensionality D . Instead, the particular choices of the matrix H_0 and interaction coefficients $J_{a,b}^{l_1, l_2}$ in Eq. (1) are irrelevant for p_{cr} (so long as the network connectivity is unchanged). The critical values of the filling fraction δ_{cr} where a transition between transporting and non-transporting regimes occurs is related to the critical

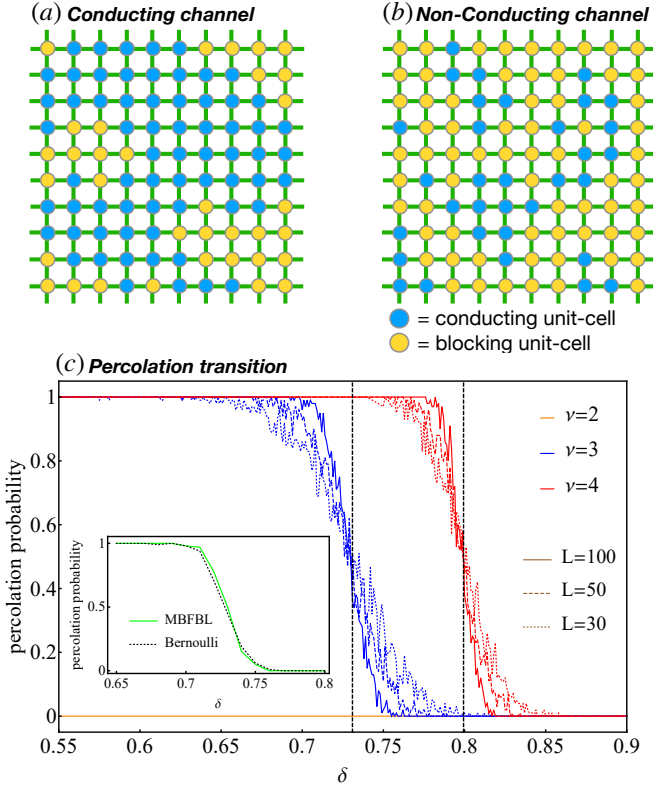


FIG. 3. (a) Typical state from a conducting channel in an equispaced square MBFBL network Eq. (1) with FD \hat{H}_{int} (green lines) and SD \hat{H}_{sp} (circles) distinguished in conducting unit cells (blue) and blocked unit cells (orange). (b) Same as (a) for a non-conducting subspace. (c) Percolation probability versus filling fraction δ for different system sizes L and number of sites per unit cell ν calculated using 100 Monte-Carlo samples for each point. Vertical dashed lines – critical filling fraction given by Eq. (5). Inset: comparison of Bernoulli and MBFBL percolation models for $\nu = 3$, $L = 100$.

probability p_{cr} through

$$1 - \delta_{\text{cr}}^\nu - (1 - \delta_{\text{cr}})^\nu = p_{\text{cr}}. \quad (5)$$

We start with the simplest case and consider a $D = 2$ Hamiltonian \hat{H} (1) arranged as a square lattice. In Fig. 3 we schematically illustrate conducting channels (a) and states from non-conducting subspace (b). The site-percolation critical value in this network is $p_{\text{cr}} \sim 0.59$ [54]. In Fig. 3(c) we show the numerically computed percolation probability as a function of the filling fraction δ for several system sizes L and number of sites per unit cell ν . The inset of Fig. 3(c) compares the percolation probabilities calculated from the Bernoulli percolation model and from the direct sampling of the fermionic Hilbert space. The results are in excellent agreement justifying the application of the Bernoulli model. For $\nu = 2$ the probability that a unit cell is conducting is $p \leq 0.5$ for any δ , with the maximum $p = 0.5$ being reached at $\delta = 0.5$ – hence, the transition value $p_{\text{cr}} \sim 0.59$ is never

reached, the network never undergoes percolation transition and global transport is suppressed for all filling fractions δ . Numerical simulations confirm this conclusion for $\nu = 2$. For $\nu = 3, 4$ numerical simulations give clear evidences of a percolation transition upon varying δ , again in excellent agreement with the critical values predicted by Eq. (5).

In $D = 2$ the majority of lattices – kagome, honeycomb, octagon – have critical values $p_{\text{cr}} \gtrless 0.5$ [55]. Exceptions include networks with further than nearest-neighbor terms [56], chimera [57], and triangular lattice [58]. Hence, in two dimensions, most of $\nu = 2$ MBFBL networks \hat{H} avoid percolation transition (and therefore any transport is absent) since the maximum probability of a unit cell to be conducting is $p = 0.5$. As D increases, the critical transition p_{cr} in a given class of lattices typically decreases: for example $D \geq 3$ hyper-cubic networks \hat{H} percolation transition occurs for any $\nu \geq 2$ [53]. However, exotic networks on which \hat{H} avoid percolation transition exist: for instance, $\nu = 2$ MBFBL networks on 3D cubic-oxide or 3D silicon-dioxide [59, 60].

Geometric percolation theory yields regions of filling fraction where the number of states from conducting channels is dominating over those from the non-conducting ones. However, quantum transport in these regions can still be hindered due to several additional factors, that become clear once mappings to spin models, that generalize the $D = 1$ case are considered. These factors follow from the local constraints $\{\hat{I}_1\}$. Firstly, as discussed for the spin mapping within the conducting subspace in $D = 1$, distributions of particles in the conducting cells can generate disorder in the interactions, the local spin fields (for $\nu \geq 3$), and even the spin lengths (for $\nu \geq 4$). Secondly, percolating clusters in conducting channels have in general a highly irregular fractal structure [61], yielding edge scattering. This source of scattering – already present in classical percolation – is in our context further amplified by the inhomogeneous arrangements of blocking cells in the network. This yields additional, effectively random fields in the spin model in the conducting cells at the edges of the percolating cluster. Finally, let us point out that the existence of dead-end bonds which fully reflect waves and lead to an effective increase of the percolation threshold with respect to the classical one – a phenomenon called *quantum percolation* [62, 63] – has been demonstrated for single-particle quantum percolation clusters. Thus, the classical values of critical probability p_{cr} discussed above could only be a lower bound on the effective quantum threshold values for the MBFBL networks.

Conclusions and Perspectives — In this work we studied transport features of translationally invariant interacting many-body flatband (MBFBL) networks [38–40]. While charges are strictly confined in these models due to local constraints, heat is in principle allowed to flow along conducting channels – leading to site-percolation

transitions in the networks. We found that in 1D the number of conducting channels either vanishes or decays exponentially with the system size, hence suppressing any transport. In higher dimensions, the number of conducting channels can undergo a percolation transition upon tuning the filling fraction δ , potentially triggering heat transport. However, the presence of the transition depends on the network type, the number of single-particle energy bands ν , and the dimensionality D . While we explicitly verified this conclusions for the case of spinless fermions, these results hold for any type of many-body statistics.

Our analysis – rooted in geometric percolation theory, alongside recent findings of localization/delocalization transition in 2D quantum link models [19] – overcomes the complexity typical of $D \geq 2$ many-body systems which render their computational analysis impractical nowadays. Importantly, we highlight classes of disorder-free many-body systems in two and higher spatial dimensions where any type of transport is completely suppressed for any filling fraction δ . Even in those networks that feature conducting phases, quantum transport is hurdled and potentially halted by effective disorder and edge effects resulting from the local constraints. Exploring these quantum effects and investigating the distinction between classical and quantum percolation transitions [62, 63] are crucial future developments, which may have important repercussions for the research in the field of quantum transport. These results and open quests emphasize MBFBL networks as experimentally realizable [64–66] valid platforms to explore novel phenomena in quantum systems – highlighting jointly with Refs. [29–40] the progressively growing relevance of flatbands in the realm of many-body physics.

Acknowledgments — This work was supported by the Institute for Basic Science (Project number IBS-R024-D1). We thank Ivan Khaymovich for helpful discussions.

* Corresponding author
igrvak@gmail.com

† Corresponding author
cdanieli@pks.mpg.de

‡ Corresponding author
aalexei@ibs.re.kr

§ Corresponding author
sergejflach@googlemail.com

- [1] L. Fleishman and P. W. Anderson, “Interactions and the anderson transition,” *Phys. Rev. B* **21**, 2366–2377 (1980).
- [2] Boris L. Altshuler, Yuval Gefen, Alex Kamenev, and Leonid S. Levitov, “Quasiparticle lifetime in a finite system: A nonperturbative approach,” *Phys. Rev. Lett.* **78**, 2803–2806 (1997).
- [3] Ph. Jacquod and D. L. Shepelyansky, “Emergence of quantum chaos in finite interacting fermi systems,” *Phys. Rev. Lett.* **79**, 1837–1840 (1997).
- [4] I. V. Gornyi, A. D. Mirlin, and D. G. Polyakov, “Interacting electrons in disordered wires: Anderson localization and low- t transport,” *Phys. Rev. Lett.* **95**, 206603 (2005).
- [5] D.M. Basko, I.L. Aleiner, and B.L. Altshuler, “Metal–insulator transition in a weakly interacting many-electron system with localized single-particle states,” *Ann. Phys.* **321**, 1126 – 1205 (2006).
- [6] Dmitry A. Abanin and Zlatko Papić, “Recent progress in many-body localization,” *Ann. Phys.* **529**, 1700169 (2017).
- [7] Dmitry A. Abanin, Ehud Altman, Immanuel Bloch, and Maksym Serbyn, “Colloquium: Many-body localization, thermalization, and entanglement,” *Rev. Mod. Phys.* **91**, 021001 (2019).
- [8] Mauro Schiulaz, Alessandro Silva, and Markus Müller, “Dynamics in many-body localized quantum systems without disorder,” *Phys. Rev. B* **91**, 184202 (2015).
- [9] Merlijn van Horssen, Emanuele Levi, and Juan P. Garrahan, “Dynamics of many-body localization in a translation-invariant quantum glass model,” *Phys. Rev. B* **92**, 100305 (2015).
- [10] Manuel Pino, Lev B. Ioffe, and Boris L. Altshuler, “Non-ergodic metallic and insulating phases of Josephson junction chains,” *PNAS* **113**, 536–541 (2016).
- [11] James M Hickey, Sam Genway, and Juan P Garrahan, “Signatures of many-body localisation in a system without disorder and the relation to a glass transition,” *Journal of Statistical Mechanics: Theory and Experiment* **2016**, 054047 (2016).
- [12] Rubem Mondaini and Zi Cai, “Many-body self-localization in a translation-invariant hamiltonian,” *Phys. Rev. B* **96**, 035153 (2017).
- [13] M. Schulz, C. A. Hooley, R. Moessner, and F. Pollmann, “Stark many-body localization,” *Phys. Rev. Lett.* **122**, 040606 (2019).
- [14] A. Smith, J. Knolle, D. L. Kovrizhin, and R. Moessner, “Disorder-free localization,” *Phys. Rev. Lett.* **118**, 266601 (2017).
- [15] A. Smith, J. Knolle, R. Moessner, and D. L. Kovrizhin, “Absence of ergodicity without quenched disorder: From quantum disentangled liquids to many-body localization,” *Phys. Rev. Lett.* **119**, 176601 (2017).
- [16] Adam Smith, Johannes Knolle, Roderich Moessner, and Dmitry L. Kovrizhin, “Dynamical localization in \mathbb{Z}_2 lattice gauge theories,” *Phys. Rev. B* **97**, 245137 (2018).
- [17] Marlon Brenes, Marcello Dalmonte, Markus Heyl, and Antonello Scardicchio, “Many-body localization dynamics from gauge invariance,” *Phys. Rev. Lett.* **120**, 030601 (2018).
- [18] Oliver Hart, Sarang Gopalakrishnan, and Claudio Castelnovo, “Logarithmic entanglement growth from disorder-free localisation in the two-leg compass ladder,” (2020), [arXiv:2009.00618 \[cond-mat.str-el\]](https://arxiv.org/abs/2009.00618).
- [19] P. Karpov, R. Verdel, Y.-P. Huang, M. Schmitt, and M. Heyl, “Disorder-free localization in an interacting 2d lattice gauge theory,” *Phys. Rev. Lett.* **126**, 130401 (2021).
- [20] Thorsten B. Wahl, Arijeet Pal, and Steven H. Simon, “Signatures of the many-body localized regime in two dimensions,” *Nature Physics* **15**, 164–169 (2019).
- [21] Jae-yoon Choi, Sebastian Hild, Johannes Zeiher, Peter Schauf, Antonio Rubio-Abadal, Tarik Yefsah, Vedika Khemani, David A. Huse, Immanuel Bloch, and

- Christian Gross, “Exploring the many-body localization transition in two dimensions,” *Science* **352**, 1547–1552 (2016).
- [22] Wojciech De Roeck and Franois Huveneers, “Stability and instability towards delocalization in many-body localization systems,” *Phys. Rev. B* **95**, 155129 (2017).
- [23] Oleg Derzhko, Johannes Richter, and Mykola Maksymenko, “Strongly correlated flat-band systems: The route from heisenberg spins to hubbard electrons,” *Int. J. Mod. Phys. B* **29**, 1530007 (2015).
- [24] Daniel Leykam, Alexei Andreanov, and Sergej Flach, “Artificial flat band systems: from lattice models to experiments,” *Adv. Phys.: X* **3**, 1473052 (2018).
- [25] Daniel Leykam and Sergej Flach, “Perspective: Photonic flatbands,” *APL Photonics* **3**, 070901 (2018).
- [26] Julien Vidal, R my Mosseri, and Benoit Douot, “Aharonov-Bohm cages in two-dimensional structures,” *Phys. Rev. Lett.* **81**, 5888–5891 (1998).
- [27] Julien Vidal, Benoit Douot, R my Mosseri, and Patrick Butaud, “Interaction induced delocalization for two particles in a periodic potential,” *Phys. Rev. Lett.* **85**, 3906–3909 (2000).
- [28] Benoit Douot and Julien Vidal, “Pairing of cooper pairs in a fully frustrated josephson-junction chain,” *Phys. Rev. Lett.* **88**, 227005 (2002).
- [29] Murad Tovmasyan, Sebastiano Peotta, Long Liang, P ivi T rm , and Sebastian D. Huber, “Preformed pairs in flat bloch bands,” *Phys. Rev. B* **98**, 134513 (2018).
- [30] Simon Tilleke, Mirko Daumann, and Thomas Dahm, “Nearest neighbour particle-particle interaction in fermionic quasi one-dimensional flat band lattices,” *Z. Naturforsch. A* **75**, 20190371 (2020).
- [31] Carlo Danieli, Alexei Andreanov, Thudiyangal Mithun, and Sergej Flach, “Quantum caging in interacting many-body all-bands-flat lattices,” (2020), [arXiv:2004.11880 \[cond-mat.quant-gas\]](#).
- [32] Oliver Hart, Giuseppe De Tomasi, and Claudio Castelnovo, “From compact localized states to many-body scars in the random quantum comb,” *Phys. Rev. Research* **2**, 043267 (2020).
- [33] Paul A. McClarty, Masudul Haque, Arnab Sen, and Johannes Richter, “Disorder-free localization and many-body quantum scars from magnetic frustration,” *Phys. Rev. B* **102**, 224303 (2020).
- [34] Yoshihito Kuno, Tomonari Mizoguchi, and Yasuhiro Hatsugai, “Flat band quantum scar,” *Phys. Rev. B* **102**, 241115 (2020).
- [35] Mirko Daumann, Robin Steinigeweg, and Thomas Dahm, “Many-body localization in translational invariant diamond ladders with flat bands,” (2020), [arXiv:2009.09705 \[cond-mat.stat-mech\]](#).
- [36] Rishabh Khare and Sayan Choudhury, “Localized dynamics following a quantum quench in a non-integrable system: an example on the sawtooth ladder,” *Journal of Physics B: Atomic, Molecular and Optical Physics* **54**, 015301 (2020).
- [37] Carlo Danieli, Alexei Andreanov, and Sergej Flach, “Many-body localization transition from flatband fine-tuning,” (2021), [arXiv:2104.11055 \[cond-mat.stat-mech\]](#).
- [38] Carlo Danieli, Alexei Andreanov, and Sergej Flach, “Many-body flatband localization,” *Phys. Rev. B* **102**, 041116(R) (2020).
- [39] Yoshihito Kuno, Takahiro Orito, and Ikuo Ichinose, “Flat-band many-body localization and ergodicity breaking in the Creutz ladder,” *New J. Phys.* **22**, 013032 (2020).
- [40] Takahiro Orito, Yoshihito Kuno, and Ikuo Ichinose, “Exact projector hamiltonian, local integrals of motion, and many-body localization with symmetry-protected topological order,” *Phys. Rev. B* **101**, 224308 (2020).
- [41] Sthitadhi Roy, J. T. Chalker, and David E. Logan, “Percolation in fock space as a proxy for many-body localization,” *Phys. Rev. B* **99**, 104206 (2019).
- [42] Sthitadhi Roy, David E. Logan, and J. T. Chalker, “Exact solution of a percolation analog for the many-body localization transition,” *Phys. Rev. B* **99**, 220201 (2019).
- [43] P. Prelov sek, M. Mierzejewski, J. Krsnik, and O. S. Bari i, “Many-body localization as a percolation phenomenon,” *Phys. Rev. B* **103**, 045139 (2021).
- [44] Let us observe that if H_0 in Eq. (1) is diagonal, then every particle number operator $\hat{n}_{l,a}$ for any l and a is conserved – hence fully suppressing heat transport as well.
- [45] Carlo Danieli, Alexei Andreanov, Thudiyangal Mithun, and Sergej Flach, “Nonlinear caging in all-bands-flat lattices,” (2020), [arXiv:2004.11871 \[cond-mat.quant-gas\]](#).
- [46] R. B. Stinchcombe, “Ising model in a transverse field. i. basic theory,” *Journal of Physics C: Solid State Physics* **6**, 2459–2483 (1973).
- [47] In Eq. (3) we neglected the constant energy shift terms which do not impact the dynamics of the system.
- [48] For a conducting island with $1 \leq l \leq M$ conducting cells, the boundary terms in Eq. (3) read $\frac{1}{4}[(\hat{I}_0 - 1)\hat{\sigma}_1^z + (1 - \hat{I}_{M+1})\hat{\sigma}_M^z]$, where \hat{I}_0, \hat{I}_{M+1} are the particles number operators in unit cells $l = 0, M + 1$.
- [49] Ke-Wei Sun, Chen Wang, and Qing-Hu Chen, “Heat transport in an open transverse-field ising chain,” *EPL (Europhysics Letters)* **92**, 24002 (2010).
- [50] The two forms of H_0 are equal for specific cases – e.g. with constant diagonal entrees s and equal non-zero off-diagonal entrees t .
- [51] Yevgeny Bar Lev, David R. Reichman, and Yoav Sagi, “Many-body localization in system with a completely delocalized single-particle spectrum,” *Phys. Rev. B* **94**, 201116 (2016).
- [52] Hugo Duminil-Copin, “Sixty years of percolation,” in *Proceeding of the International Congress* (World Scientific, 2018).
- [53] Abbas Ali Saberi, “Recent advances in percolation theory and its applications,” *Phys. Rep.* **578**, 1–32 (2015), recent advances in percolation theory and its applications.
- [54] Jesper Lykke Jacobsen, “Critical points of potts and $o(n)$ models from eigenvalue identities in periodic temperley–lieb algebras,” *J. Phys. A: Math. Theor.* **48**, 454003 (2015).
- [55] Paul N. Suding and Robert M. Ziff, “Site percolation thresholds for archimedean lattices,” *Phys. Rev. E* **60**, 275–283 (1999).
- [56] Mariusz Majewski and Krzysztof Malarz, “Square lattice site percolation thresholds for complex neighbourhoods,” [arXiv preprint cond-mat/0609635](#) (2006).
- [57] O. Melchert, Helmut G. Katzgraber, and M. A. Novotny, “Site- and bond-percolation thresholds in $K_{n,n}$ -based lattices: Vulnerability of quantum annealers to random qubit and coupler failures on chimera topologies,” *Phys. Rev. E* **93**, 042128 (2016).
- [58] Stanislav Smirnov, “Critical percolation in the plane: conformal invariance, cardy’s formula, scaling limits,”

- Comptes Rendus de l'Académie des Sciences - Series I - Mathematics **333**, 239–244 (2001).
- [59] Jonathan Tran, Ted Yoo, Shane Stahlheber, and Alex Small, “Percolation thresholds on three-dimensional lattices with three nearest neighbors,” *J. Stat. Mech.* **2013**, P05014 (2013).
 - [60] Ted Y Yoo, Jonathan Tran, Shane P Stahlheber, Carina E Kaainoa, Kevin Djepang, and Alexander R Small, “Site percolation on lattices with low average coordination numbers,” *J. Stat. Mech.* **2014**, P06014 (2014).
 - [61] Hans J. Herrmann and H. Eugene Stanley, “Building blocks of percolation clusters: Volatile fractals,” *Phys. Rev. Lett.* **53**, 1121–1124 (1984).
 - [62] Yigal Meir, Amnon Aharony, and A Brooks Harris, “Quantum percolation,” in *Scaling Phenomena in Disordered Systems* (Springer, 1991) pp. 381–385.
 - [63] Gerald Schubert and Holger Fehske, “Quantum percolation in disordered structures,” in *Quantum and Semi-classical Percolation and Breakdown in Disordered Solids* (Springer, 2009) pp. 1–28.
 - [64] Kejie Fang, Zongfu Yu, and Shanhui Fan, “Realizing effective magnetic field for photons by controlling the phase of dynamic modulation,” *Nature Photonics* **6**, 782–787 (2012).
 - [65] Seabrata Mukherjee, Marco Di Liberto, Patrik Öhberg, Robert R. Thomson, and Nathan Goldman, “Experimental observation of Aharonov-Bohm cages in photonic lattices,” *Phys. Rev. Lett.* **121**, 075502 (2018).
 - [66] Sergey Gladchenko, David Olaya, Eva Dupont-Ferrier, Benoit Douçot, Lev B. Ioffe, and Michael E. Gershenson, “Superconducting nanocircuits for topologically protected qubits,” *Nature Phys.* **5**, 48–53 (2009).